*URSI GASS 2023, Sapporo, Japan, 19 – 26 August 2023*

# Observations and statistics of the plasmasphere boundaries from the Van Allen Probes

J.-F. Ripoll* [(1)(2)], S. A. Thaller[(3)], D. P. Hartley[(4)], G. S. Cunningham[(5)], V. Pierrard[(6,7)], W. S. Kurth[(4)], C. A. Kletzing[(4)], J. R. Wygant[(8)]

(1) CEA, DAM, DIF, F-91297 Arpajon, France; e-mail: jean-francois.ripoll@cea.fr; thomas.farges@cea.fr
(2) UPS, CEA, LMCE, 91680 Bruyères-le-Châtel, France
(3) Orion Space Solutions, Louisville, CO, USA; scott.thaller@orionspace.com
(4) Department of Physics and Astronomy, University of Iowa, Iowa City, IA, USA; david-hartley@uiowa.edu; craig-kletzing@uiowa.edu; william-kurth@uiowa.edu
(5) Los Alamos National Laboratory, Los Alamos, New Mexico, USA; e-mail: cunning@lanl.gov
(6) Royal Belgian Institute for Space Aeronomy, Brussels, B-1180, Belgium; viviane.pierrard@aeronomie.be
(7) Center for Space Radiations, ELI-C, Université Catholique de Louvain, Louvain-La-Neuve, Belgium
(8) School of Physics and Astronomy, University of Minnesota, Minneapolis, Minnesota, USA

## Abstract

We deduce the cold electron plasma density from NASA Van Allen Probes measurements throughout 2012–2019. We then extract two of the plasmasphere boundaries. We first use the gradient method for locating the plasmapause at $L_{pp}$ and, then, the 100 $cm^{-3}$ density threshold for the plasmasphere outer edge located at $L_{100}$. The sharp gradient of the plasmapause is only defined in 53% of cases, while $L_{100}$ is defined for ~85% of cases. Differences and similarities between $L_{pp}$ and $L_{100}$ are discussed. $L_{100}$ is demonstrated to bound the plasmasphere at large L-shell in the dusk where $L_{pp}$ gradients often lack. We generate new empirical density models of the plasmasphere boundaries binned by L-shell, magnetic local time (MLT), and the maximum of the Kp index over 24 hours (Kp*).

## 1 Introduction

The Earth's plasmasphere is a region of plasma extending out from the ionized upper part of the atmosphere to distances of L~2–6 Earth Radii. The plasmapause is generally defined as an abrupt decrease in cold electron density (~1 eV), when it exists, between the dense (> ~100 $cm^{-3}$) plasmasphere and the low-density (<~10 $cm^{-3}$) plasmatrough region [1, 2]. Whistler-mode waves that energize radiation belt particles (e.g., chorus) are found outside the plasmasphere. Inside the plasmasphere, different whistler-mode waves (e.g., hiss) exist and cause radiation belt particles to precipitate into Earth's atmosphere by wave-particle interaction. (See radiation belt physics review in [3]). Therefore, models predicting the radiation belt's dynamics require the knowledge of the plasmapause location for predicting the radiation dose encountered by spacecraft orbiting through the radiation belts.

In this summary article, we present statistics of the Earth's plasmasphere boundaries in L using two methods; either as a gradient, $L_{pp}$ (when it exists), or as a dense outer edge of the plasmasphere close to the 100 $cm^{-3}$ density level, $L_{100}$. Comparing the position of $L_{pp}$ and $L_{100}$ (when both exist) will allow us to conclude whether or not both boundaries converge toward the plasmapause location. We then derive empirical models of both the $L_{pp}$ and the $L_{100}$ locations with a parametrization with respect to magnetic local time (MLT) and the maximum of Kp over the previous 24 hours, noted $Kp^*$.

## 2 The cold electron density as observed from the Van Allen Probes

The cold electron density is first extracted from the Electric and Magnetic Field Instrument Suite and Integrated Science (EMFISIS) Waves instrument [4] upper hybrid frequency, $f_{UHR}$ [5]. Cold plasma densities are also determined using the spacecraft floating potential [6] measured by the Electric Field and Waves (EFW) instrument [7]. Here, EFW and EMFISIS densities are used for the whole Van Allen Probe B mission, from 26 September 2012 to 16 July 2019 (referred as EFW and EMFISIS data).

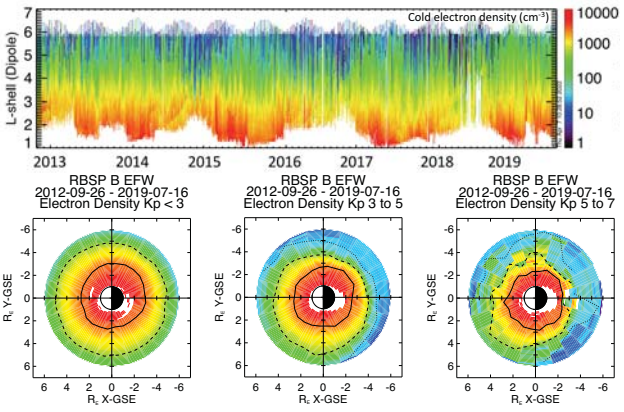


**Figure 1.** (top) The Electric Field and Waves (EFW) electron plasma density (log10 in $cm^{-3}$) from Van Allen Probes B during the whole mission. (bottom) The electron plasma density binned by (L, MLT) for 3 Kp bins of

geomagnetic activity. Level lines of (solid) 1,000 $cm^{-3}$, (long dashed) 100 $cm^{-3}$, (dashed) 10 $cm^{-3}$ are indicated.

Figure 1(top) shows the EFW density plotted for the whole Van Allen Probe B mission. The L-shell L refers here to the dipole L. Erosion of the plasmasphere is commonly visible down to L~3 during geomagnetic storms. Plasmaspheric densities of 100 $cm^{-3}$ can extend beyond L~6 during geomagnetic quiet times. The transition region between 10 and 100 $cm^{-3}$ can exceed ~1 L in width.
Figure 1(bottom) illustrates the state of the plasmasphere for 3 bins in Kp index spanning quiet to high levels of geomagnetic activity, a range of conditions that models intend to reproduce. During quiet times, the plasmasphere is approximately circular in shape around the Earth. It can commonly expand out up to L~5.5. With increasing activity, the plasmasphere evolves to become more asymmetric in shape. Density structures form in the morning and afternoon sectors. The increase of geomagnetic activity produces a general erosion of the plasmasphere on the dayside. We also see an outward expansion of the plasma density in the dusk sector. In some of the night-morning sectors, we see an increase of density due to detached plasma regions rolling and wrapping around Earth.

## 3 Comparison of $L_{pp}$ and $L_{100}$ plasmasphere boundaries

The dense outer edge of the plasmasphere, $L_{100}$, is defined by the L value at a density threshold of ~100 $cm^{-3}$ following [1]. For each half orbit, we search for the first minimum of the density below the 100 $cm^{-3}$ threshold and in the (30, 100) range using the 0.1 L binned density data. The plasmapause, $L_{pp}$, is determined using the original density gradient method from [2], defined as a variation of the density by a factor 5 within half L for each half-orbit. This method is the most common (e.g.,[8]) and is here applied to the 0.1 L binned EFW and EMFISIS densities shown in Figure 1. More details on the method can be found in [9]. A first result is the sharp gradient of the plasmapause is defined only in 53% of cases, while $L_{100}$ is defined for ~85% of cases, on a total of ~14,000 half orbits. Figure 2 shows a direct comparison between the threshold, $L_{100}$, and gradient, $L_{pp}$, methods for each half-orbit when both are defined.

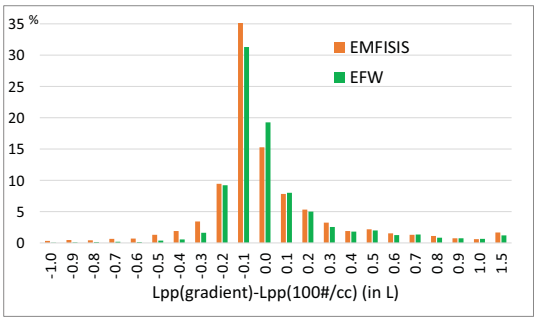


**Figure 2.** Probability of the difference between the threshold ($L_{100}$) and gradient ($L_{pp}$) methods given in L value and computed for both EFW and EMFISIS instruments.

We find 53% of differences ($L_{pp} - L_{100}$) are within [−0.1 L, 0.1 L], representing the minimal size of the L-shell bin. There are 69% within [−0.2 L, 0.2 L], 77% within [−0.3 L, 0.3 L], and 86% within [−0.5 L, 0.5 L]. The signed density difference ($n_{pp} - n_{100}$) is ±100 $cm^{-3}$ for 75% of cases. This difference is in between −100 and +300 $cm^{-3}$ for 97% of cases.

## 4 $L_{pp}$ and $L_{100}$ variations with L-shell and MLT

A $L_{100}$ value below L=3 represents 2% of the cases (with only three events falling below L = 2 ± 0.25). 95% of $L_{100}$ are between 3.25 and 5.75 and 50% identifications occur between 4.25 and 5.25, with a quite flat distribution in L. $L_{100}$ data reaches 5.5 ± 0.25 commonly in 18% of cases, associated with quiet times. They reach up to L = 6 ± 0.25 in 5% of cases. Values above L~6 are limited by the RBSP apogee. Such a far extension confirms the influence of the plasmasphere, through the whistler-mode hiss wave power it contained, far inside the outer radiation belt [10, 11]. Figure 3 (red histogram) shows the general distribution of $L_{100}$ with respect of L-shell. Other histogram colors show how the distributions of $L_{100}$ reaches lower L-shells as $Kp^*$ increases (from yellow to black), with always a large spread over L-shell of ~2 L for a given $Kp^*$ bin

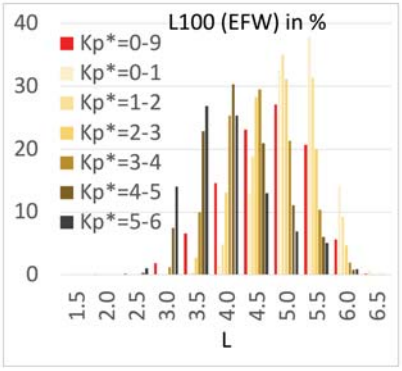


**Figure 3.** Distributions of $L_{100}$ (in % of data) versus L-shell and $Kp^*$.

Figure 4 provides EMFISIS MLT distributions of both $L_{pp}$ and $L_{100}$. The gradient method finds more plasmapause crossings where erosion is strongest in the night/dawn sectors and less where extended or diluted plasmasphere occurs due to expansion and plume dynamics in the noon and dusk sectors. This confirms a bias of the gradient method in favor of the night/dawn side. Statistics, which are limited to data for which both $L_{pp}$ and $L_{100}$ are defined (in yellow), show similar behavior for $L_{pp}$ and $L_{100}$ in MLT attesting the gradient of the plasmapause is close to the 100 $cm^{-3}$ level (as generally shown in Figure 2). However, statistics restricted to data for which $L_{100}$ is defined but the $L_{pp}$ is not defined (plotted in green in Figure 4) show the threshold method offers a boundary peaked on the dusk side. Statistics generated from EFW data show similar

behaviors (not shown). Thus, the 100 $cm^{-3}$ outer edge of the plasmasphere encompasses the plasmapause when a density gradient exists (~1 case out of two), provides a clear L-shell limit in the dusk sector for the diluted plasmasphere (where gradients are most often lacking). It also avoids a bias of the gradient method statistics on the night/dawn side due to lacking gradients in the dusk sector.

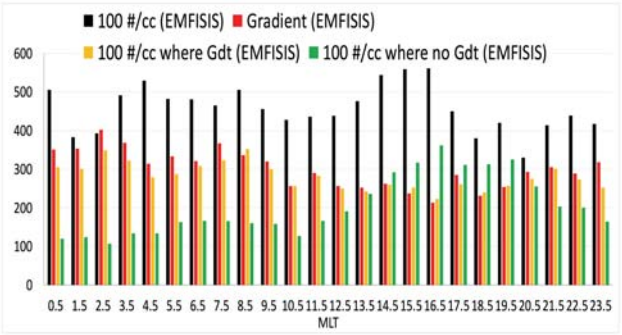


**Figure 4.** Distributions of the electron density in magnetic local time (MLT) (in #) at the 100 $cm^{-3}$ ($L_{100}$) and gradient ($L_{pp}$) positions (EMFISIS data).

## 5 Empirical models of $L_{pp}$ and $L_{100}$

Statistics are used to create a new generation of empirical plasmapause models with respect to L-shell, MLT, and $Kp^*$ shown in Figure 5. We follow the approach of similar older models based on other satellite data (e.g., [2], [8]). Former existing plasmapause models are reviewed in [12]. As pointed out, this type of models are commonly used in radiation belt codes for separating hiss and chorus waves and better organize the whistler-mode waves inside and outside of the plasmasphere [3]. This has drastic influence on the repartition of acceleration and loss. Both the mean value and the standard deviation are generated.

Sorting the plasmapause and $L_{100}$ by $Kp^*$, we find a linear dependence for both $L_{100}$ and $L_{pp}$ defined as $b - aKp^*$, in agreement with [8]. For $L_{100}$ and using EFW data [9], we find:

a = (0.36/0.38/0.31/0.25/0.34)

b=(5.62/5.57/5.59/5.48/5.51)

For $L_{pp}$ (gradient method) and using EFW data [9], we find:

a = (0.34/0.41/0.34/0.21/0.38)

b = (5.63/5.62/5.48/5.27/5.47)

Each parameter is defined at centered MLT= (00/06/12/18/All) for $Kp^* \leq 6$. $L_{100}$ becomes MLT-dependent for $Kp^* > 3$, which justifies introducing a MLT dependence in the new models. The standard deviation of $L_{100}$ is ~±0.5 L and minimal for quiet times ($Kp^*<3$). The standard deviation increases with geomagnetic activity, up to ~±1 L. There is a large variability with geomagnetic activity, limiting the model validity up to Kp*=6. The $L_{pp}$ standard deviation is much larger than the one of the $L_{100}$. This is particularly pronounced for low activity and in the dusk sector. This is due to lack of gradient for these condition and location as well as gradients that may be identified in very low-density regions (below 20 #/cc).

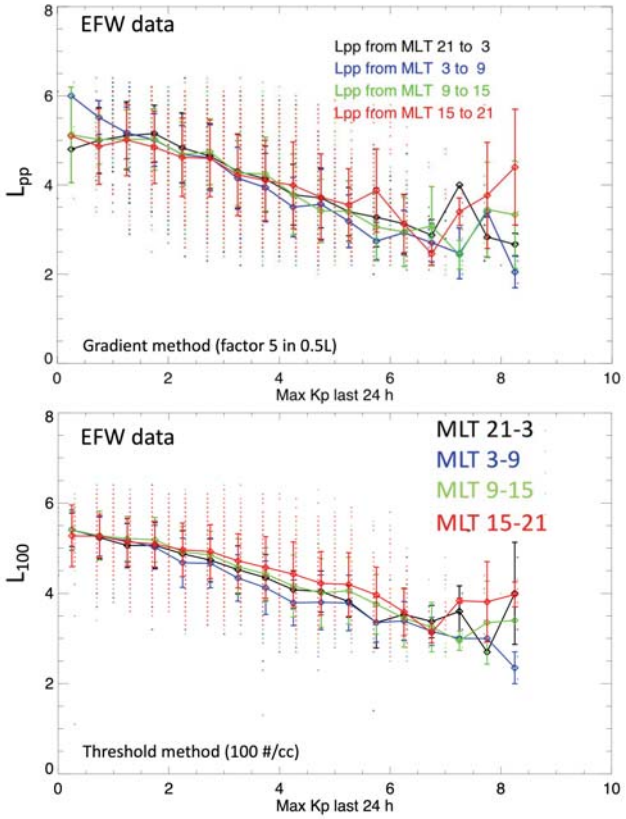


**Figure 5.** Empirical models of the (top) plasmapause position $L_{pp}$ computed by a gradient method and (bottom) the 100 $cm^{-3}$ plasmasphere outer edge, $L_{100}$, computed by a threshold method. Models are defined for 4 MLT sectors as a function of $Kp^*$. Dots indicate individual values. Bars indicate the standard deviation.

## 6 Conclusions

We statistically study the Earth's plasmasphere boundaries through the plasmapause location defined by a gradient at Lpp and the 100 $cm^{-3}$ threshold for the plasmasphere dense outer edge at $L_{100}$ using both EFW spacecraft floating potential and EMFISIS fUHR cold electron plasma densities onboard Van Allen Probes. Our results confirm Carpenter's knee occurs in the vicinity of ~100 $cm^{-3}$. This supports a possible labeling of the outer edge of the plasmasphere at ~100 $cm^{-3}$ as the plasmapause. Statistics are used to create a new generation of empirical plasmapause models with respect to L-shell, MLT, and $Kp^*$. Mean value and standard deviation are generated for uncertainty quantification. The plasmapause empirical models are provided here, with more dependences in [9] and through text files which can be downloaded from [13].

## Acknowledgements

The authors thank the EFW and EMFISIS teams of the Van Allen Probes mission for their support. The authors thank the National Science Foundation Geospace Environment Modeling Project 2040708. The authors thank the

International Space Sciences Institute (ISSI) and the participants in a 2020 ISSI workshop for the project "Radiation belts physics." The work of J.-F.R. and G.S.C. was performed under the auspices of an agreement between Commissariat à l'Energie Atomique, Direction des Applications Militaires (CEA/DAM) and National Nuclear Security Administration, Defense Program (NNSA/DP) on cooperation on fundamental science. D.P.H. acknowledges NASA Grant 80NSSC20K1324. V.P. acknowledges the Horizon 2020 PITHIA-NRF grant agreement No. 101007599.

## References

[1] Carpenter, D. L. (1966). Whistler studies of the plasmapause in the magnetosphere: 1. Temporal variations in the position of the knee and some evidence on plasma motions near the knee. Journal of Geophysical Research, 71(3), 693–709. https://doi.org/10.1029/jz071i003p00693

[2] Carpenter, D. L., & Anderson, R. R. (1992). An ISEE/whistler model of equatorial electron density in the magnetosphere. Journal of Geophysical Research, 97(A2), 1097–1108. https://doi.org/10.1029/91JA01548

[3] Ripoll, J.-F., Claudepierre, S. G., Ukhorskiy, A. Y., Colpitts, C., Li, X., Fennell, J., & Crabtree, C. (2020). Particle dynamics in the Earth's radiation belts: Review of current research and open questions. Journal of Geophysical Research: Space Physics, 125(5), e2019JA026735. https://doi.org/10.1029/2019JA026735

[4] Kletzing, C. A., Kurth, W. S., Acuna, M., MacDowall, R. J., Torbert, R. B., Averkamp, T., et al. (2013). The electric and magnetic field instrument suite and integrated science (EMFISIS) on RBSP. Space Science Reviews, 179(1–4), 127–181. https://doi.org/10.1007/s11214-013-9993-6

[5] Kurth, W. S., De Pascuale, S., Faden, J. B., Kletzing, C. A., Hospodarsky, G. B., Thaller, S., & Wygant, J. R. (2015). Electron densities inferred from plasma wave spectra obtained by the waves instrument on Van Allen Probes. Journal of Geophysical Research: Space Physics,120(2),904–914. https://doi.org/10.1002/2014JA020857

[6] Thaller, S. A., Wygant, J. R., Dai, L., Breneman, A. W., Kersten, K., Cattell, C. A., et al. (2015). Van allen Probes investigation of the large-scale duskward electric field and its role in ring current formation and plasmasphere erosion in the 1 June 2013 storm. Journal of Geophysical Research: Space Physics, 120(6),4531–4543. https://doi.org/10.1002/2014ja020875

[7] Wygant, J. R., Bonnell, J. W., Goetz, K., Ergun, R. E., Mozer, F. S., Bale, S. D., et al. (2013). The electric field and waves instruments on the radiation belt storm Probes mission. Space Science Reviews, 179(1-4), 183–220. https://doi.org/10.1007/s11214-013-0013-7

[8] O'Brien, T. P., & Moldwin, M. B. (2003). Empirical plasmapause models from magnetic indices. Geophysical Research Letters, 30(4), 1152. https://doi.org/10.1029/2002GL016007

[9] Ripoll, J.-F., Thaller, S. A., Hartley, D. P., Cunningham, G. S., Pierrard, V., Kurth, W. S., et al. (2022). Statistics and empirical models of the plasmasphere boundaries from the Van Allen Probes for radiation belt physics. Geophysical Research Letters,49,e2022GL101402. https://doi.org/10.1029/2022GL101402

[10] Ripoll, J.-F., Loridan, V., Denton, M. H., Cunningham, G., Reeves, G., Santolík, O., et al. (2019). Observations and Fokker-Planck simulations of the L-shell, energy, and pitch angle structure of Earth's electron radiation belts during quiet times. Journal of Geophysical Research: Space Physics, 124(2),1125–1142. https://doi.org/10.1029/2018ja026111

[11] Ripoll, J.-F., Denton, M. H., Hartley, D. P., Reeves, G. D., Malaspina, D., Cunningham, G. S., et al. (2020). Scattering by whistler-mode waves during a quiet period perturbed by substorm activity. Journal of Atmospheric and Solar-Terrestrial Physics, 215, 105471. https://doi. org/10.1016/j.jastp.2020.105471

[12] Ripoll, J.-F., Pierrard, V., Cunningham, G. S., Chu X., Sorathia, K., Hartley, Thaller, S. A., S. Merkin, G. Delzanno, S. De Pascuale, A. Ukhorskiy (2023). Modeling of the electron plasma density for radiation belt physics, Review article, Frontiers in Astronomy and Space Sciences, 1096595, in press.

[13] Thaller, S. A., & Ripoll, J.-F. (2022). Plasmapause location empirical laws from spacecraft charging of the Van Allen Probes [Dataset]. Zenodo. https://doi.org/10.5281/zenodo.5889253